具網路結合功能之半導體製造集結式機台 – 總計畫(3/3)

Network Ready Semiconductor Manufacturing Cluster Tool (3/3)

計劃編號： NSC89-2218-E-002-0052
執行期限： 民國 89 年 8 月 1 日至 90 年 7 月 31 日
主持人: 呂秀雄 台灣大學機械系
共同主持人: 黃漢邦、李世光、郭瑞祥、劉致為、張培仁、張所鋐、陳正剛、呂學士、翁宗賢

☑ 出席國際學術會議心得報告及發表之論文各一份

一、中文摘要

本計畫之載具為集結式機台(Cluster Tool)，含 RTO/RTCVD 機台。一橢偏儀，一裝卸壓力艙，一機械手臂平台及一單元控制器。本計畫以此一系統為載具，發展網路式智慧型模組控制技術，建立在同一機台進行閘疊(Gate Stack)製程之技術，將橢偏儀整合於系統之技術，及建立現場(In-Situ)檢測及控制技術。本文就軟硬體架構、方法及成果做一說明。

ABSTRACT

The project deals with development of a prototype cluster tool, consisting of an RTO/RTCVD, ellipsometer, a load lock and a robot platform with a cell controller. By using the system as the vehicle, the following technologies will be developed: Gate stack process technology on a single RTO/RTCVD equipment, ellipsometer integrated in-situ inspection and process control, and intelligent network type modular controller. The framework of the system both hardware and software will be outlined, and results will be presented.

二、計畫緣由與目的

針對半導體製造之自動化及彈性製造之需求[1,2]，單晶圓製程[3,4]及多艙(Multi Chamber)或集結式(cluster)[2,5]之設備安排正擴大在半導體工廠中使用。本計畫之主要目的在於發展一集結式半導體製造機台雛型，使具現場(In-Situ)量測及控制之能力。由於半導體製造製程非常複雜，本計畫將選擇其中之一重要製程為對象，即閘疊製程。使在同一機台RTO/RTCVD 進行，即可長氧化層及多晶矽。因此，本計畫之目的在於:

1. 建立一集結式機台雛型，含機械手臂之運送平台。
2. 將本單位研發成功之橢偏儀整合於系統中為現場量測之設備。
3. 研發一網路化之單元控制器，整合機器手臂，閘疊製程設備，橢偏儀及品管模組，透過半導體之通訊標準 SECS 來完成。
4. 利用抽樣檢測及實驗設計方法建立及發展現場量測及製程控制技術。

三、研究方法及成果

(一) 研究方法

本計畫以閘疊製程為對象，擬建立一集結式機台雛型使具現場量測及控制功能，其中晶圓輸送單元以一機械手臂來完成。針對圖一及二構想之集結式機台。此集結式機台將含一RTO/RTCVD 機台，一橢偏儀，一潔靜艙，一裝卸艙(Load Lock)及中間之機械手臂搬送平台。整體系統將由一單元控制器所控制。系統並會透過網路與現有之資料庫連線，使具與網路

整合製造結合之功能。

(二)系統架構

本集結式機台之控制架構如圖三所示[6]。透過網路協調下層之機台(RTO/RTCVD, Ellispsometer)及傳輸平台(含機械手臂、裝卸艙及真空系統)及一監看系統。系統乃透過網路接收上層控制器之指令，並與配方產生工作站連接，以取得製程所需之配方。此一集結式機台單元控制器除主要監督控制工作外，亦有配方管理、統計製程控制及歷史資料記錄功能。此一單元整合檢測控制器之軟體架構如圖四所示[7]。

為了測試傳輸平台機械手臂之控制系統以及單元控制器，建立了一雛型機械手臂傳輸系統如圖五所示[8]。

(三) 集結式機台環境之發展及模式建立

應用快速應用軟體發展原則並配合 UML 圖形分析工具的使用，對單元控制器作完整的分析設計。採用 FASTech CELLworks 作為開發工具。最後經由架構在 TCP/IP 上的 HSMS 協定傳送 SECSII 訊息，建構出單元控制器和集結式機台系統運作的模擬。同時，針對使用者的需求發展出一套即時性監控模組控制器，並以斐氏圖模型來表達系統動態行為。最後在 MS Windows 98/NT 環境下並透過網路以物件導向程式語言 Visual Basic 6.0 架構出系統程式作做為模型驗證，並實現於現有之實驗型集結式平台上。

(四) 用於 12 吋晶圓製造之前段製程技術[11]

利用原有的 RTCVD 機台，將真空元件更換並加裝 Turbo pump 將可使反應腔能夠抽到 10^{-3} torr。加上流量控制、溫度控制、及未來之壓力控制，將可完成 UHV 成長之基本條件，因此機台同時具有快熱與超高真空的特性。成長之超薄氧化層製成 MOS，可當 LED 和 detector。此外，利用超高真空製程，可以使 SiO_2/Si 介面更加粗糙，對於金氧半發光二極體的發光效率有明顯的提升。對於淺接面，勢必要用到 RTA，而縮短退火時間正是研究課題，因此我們模擬晶圓降溫的曲線在有無反射體的情況下，當溫度從 900 至 1000°C 降到 600°C，時間上提早了 1.8~2.8 秒，這對於只有數秒鐘的退火大有幫助。

(五) 創新迷你橢偏儀之研製[12]

於第一年已完成先期建構橢偏儀介面及遠端使用者介面之階段目標，並於第二年研發試製低成本之微型橢偏儀，同時完成可與半導體製造集結式機台整合之橢偏儀軟硬體設計與製作，並於第三年的研究中進一步的改進了橢偏儀的功能，順利完成自我校正轉換函數的測量，且於系統上完成修改光學調校機構與光學調校方法以方便進行薄膜特性的測量，目前橢偏參數的測量結果部分取得具體的成果。計劃成果為全球首次解決於半導體製造集結式機台運用可變入射角入射光進行橢偏儀檢測時所遭遇問題之方法。系統架構圖及創新迷你橢偏儀之原型機之研製成果分別如圖六與七所示。

(六) 半導體集結式機台整合檢測及控制[7]

本計劃發展整合檢測與控制技術，其中包含了離線製程最佳化技術與線上製程控制技術。藉由整合機台、製程、材料與晶圓的資料收集，決策分析與執行，以改善機台與製程

的表現。

在第一年中，發展了合理分群技術以建立了快速熱氧化製程之非均勻度統計模型。在第二年中，發展了自我調適督導控制技術。

第三年重點為製程整合檢測與控制，具體的工作項目包含了：

1. 發展整合檢測與控制技術
2. 建立整合檢測系統雛型
3. 進行資料分析

目前第三年的目標均已完成，已發展了整合檢測與控制技術，並且建立了整合檢測系統雛型。運用時間序列與多變量統計之技術，建立了及時機台資料之模型，以作為線上機台監控之用。

四、結語

目前已建立集結式機台之軟硬體雛型試驗系統。同時，各分項工作已分別由各子計畫完成。主要之成果有集結式機台單元控制器軟體架構之建立、機械硬體系統架構之建立、現場監控系統及架構及方法之建立、完成創新型橢偏儀及與系統整合介面技術及前段製程(超薄氧化層)之實驗結果。

五、參考資料

1. Larrabee, G., et al., Manuf. Rev., v. 7, n. 3, 1997, pp. 212-226
2. McGehee, J., et al., IEEE Trans, Semicon. Manuf., v.7, n. 2, 1994, pp. 107-116
3. Hill. C., Microelectonic Eng., v. 34, n. 2, 1997, pp. 215-216
4. Wasserman, Y., Semicon. Int., v. 19, n. 6, 1996
5. Jepson, J. T., Semicon. Int., v. 19, n. 1, 1996
6. 呂秀雄、黃漢邦、張所鋐，國科會專題計畫，編號：NSC88-2218-E-002-003，研究報告，台大機械系，民國 88 年 8 月。
7. 郭瑞祥, 國科會專題計畫，編號：NSC89-2218-E-002-055, 研究報告，台大工管系，民國 90 年 8 月。
8. 張春昱, 集結式機台晶圓搬運系統之研究, 台大機械系碩士論文, 民國 89 年 6 月。
9. 鄭諭澤, 半導體廠內單元控制器於集結式機台上應用之研究, 台大機械系碩士論文, 民國 90 年 6 月。
10. 呂文瑞, 半導體廠集結式機台之監控系統研究, 台大機械系碩士論文, 民國 90 年 6 月。
11. 劉致為，國科會專題計畫，編號：NSC89-2218-E-002-054，研究報告，台大電機系，民國 90 年 8 月。
12. 李世光，國科會專題計畫，編號：NSC89-2218-E-002-053, 研究報告，台大應力所，民國 90 年 7 月。

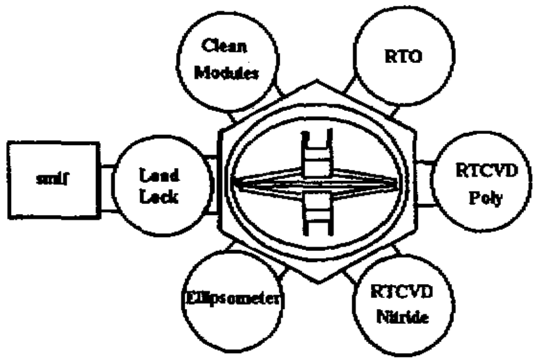

Fig. 1 A Cluster Tool Configuration

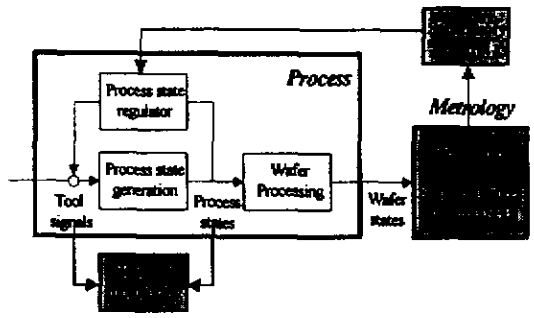

Figure 4: Integrated inspection and control

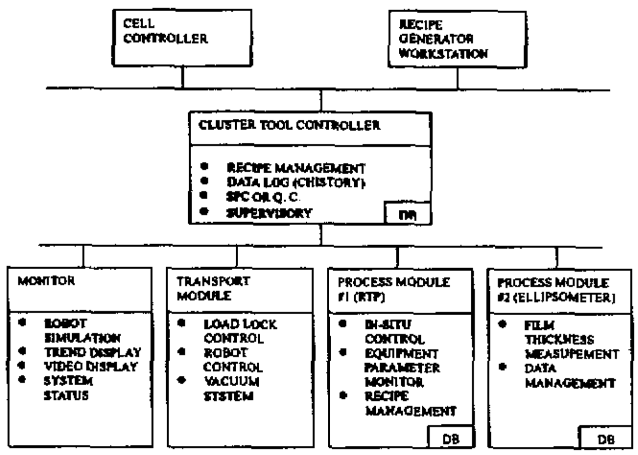

Fig. 2 System Structure

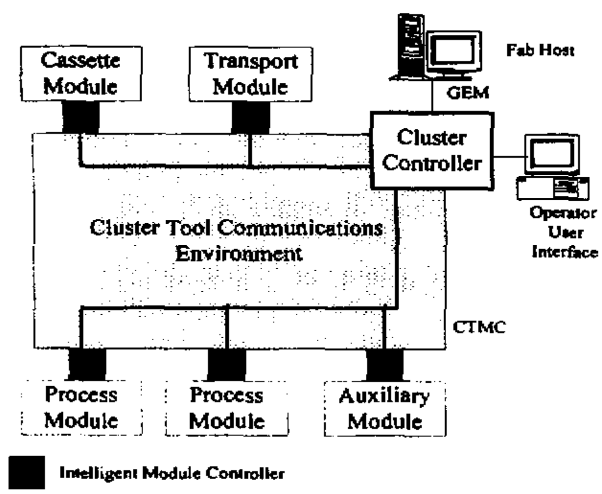

Fig. 3 Cluster Tool Control Architecture

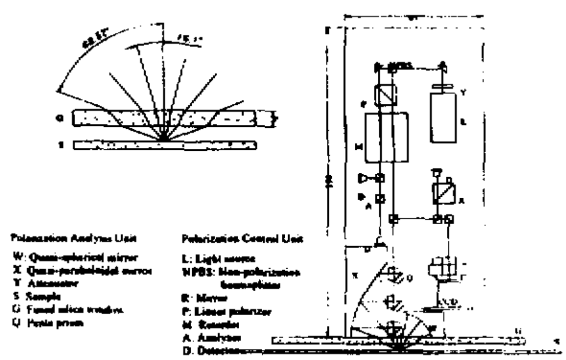

圖 6 集結式機台線上橢偏儀系統

Fig. 5 Proptorype System

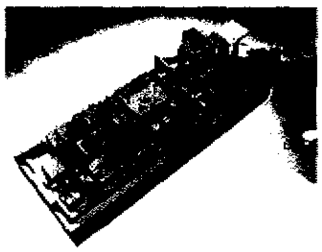

(a)光機整合 (b)電子電路與信號處理

圖 7 精偏儀機電光系統

出席國際學術會議心得報告

報告人姓名: 呂秀雄　　　　服務機關及職稱: 臺灣大學機械系教授

國科會專題研究計畫編號: NSC89-2218-E002-052

會議名稱, 時間, 地點及發表論文名稱:

I. 雷射應用於精密量測及藝術保存之國際研討會
International Symposium on Lasers in Metrology and Art Conservation
2001 年 6 月 18-22 日, Munich, Germany
論文名稱: Development and Traceability of a Multi-Functional Microscope

II. 2000 機電及智慧型機械系統國際研討會
2000 International Symposium on Mechatronics and Intelligent Mechanical System for 21 Century
2000 年 10 月 4-7 日, KyongSangNam-Do, Korea
論文名稱:
1. A Position Detection Apparatus for Ultra Precision Machine Applications
2. A Multi-Functional Microscope for Measuring Inhomogeneous Surface Profile

心得報告:

I. International Symposium on Lasers in Metrology and Art Conservation

此一研討會為 Laser 2001-World of Photonics Conference 中同時舉辦的研討會之一. 於德國慕尼黑國際會議中心舉行. 在研討會舉行之同時, 一相關之雷射應用展亦在隔鄰展出. 此為一非常重要之研討會及一重要之展覽.

在此研討會上發現有兩大發展方向值得注意. 一為奈米級量測技術 (微系統之量測) 之發展, 另一為對於 Dimensional Metrology 之可追蹤性之發展. 目前無論國內外, 對奈米技術之發展均非常重視. 此為一重要之研究領域. 然則任何製造技術之發展均需要精密量測技術之支援, 奈米技術亦不例外, 而往往量測技術決定了產品之精度及品質. 由於奈米技術需要非常高精度之量測儀器, 接觸式方式已漸難以應付需求, 故光學之非接觸式量測技術之應用就非常重要. 再此次之研討會中就有兩天有關論文之報告及討論, 有三次元量測, 線上檢測, 微機電系統振動分析用干繞儀等等. 除台大應力所李世光教授有篇論文發表外, 我國並未有相關論文發表, 顯示我國在此方面之研究有待加強.

在 Traceable Dimensional Metorlogy 方面, 亦有兩天之論文及報告, 從基本尺寸, 形狀, 到奈米量測等等. 基本上, 這一方面為有關基本標準的問題. 對於工業標準之建立非常重要. 我們的論文係在此一組發表. 另外, 我國工研院精密量測中心亦有論文發表. 無疑的, 可追蹤尺寸精密量測技術為一重要發展方向.

再此次研討會之同時, 亦順便參觀了 Laser 2001 Exhibition. 展出最新之光學器材, 及雷射之應用. 在應用方面, 以光纖通訊相關產品及雷射加工技術為主. 後者屬於高功

率雷射之應用. 由此展覽發現我國在此方面之技術亦待提升.

II. 2000 International Symposium on Mechatronics and Intelligent Mechanical System for 21 Century

此次研討會係在韓國慶尙南道昌原市舉行. 本人係受邀前往發表論文. 一共發表兩篇論文. 此爲一較小型之國際會議. 主題在於機電系統之最新發展. 由於機電系統之精度要求日趨嚴格, 傳統之機電技術漸漸無法應付要求, 光學技術乃被引進. 此次研討會上發表之論文仍以傳統之機電整合技術及應用居多. 但已有數篇報告以光機電整合爲主. 我們發表之論文亦以此爲主軸. 顯然光機電整合技術爲不可避免之發展趨勢.

由於此次研討會爲韓國慶南大學所主辦, 韓國專家學者之論文佔較多數. 由這些論文可以看出韓國在機電系統技術大致發展之概況. 其發展情形與我國之水準相近, 與日本之水準相比, 則仍落後一段距離.

Development and Traceability of A Multi-Functional Microscope

Wen-Jong Chen*[a], Chih-Kung Lee[b], Shui-Shong Lu[a], Yu-Jena Chang [a], Yu-Chiaa Chang[a], Chi-Yuana Chang[a], Shuen-Chen Shiue[b], Shu-Sheng Lee[b], Huay-Chung Liou[c]

[a]Dept. of Mechanical Engineering, National Taiwan University, Taipei, Taiwan, R.O.C
[b]Institute of Applied Mechanics, National Taiwan University, Taipei, Taiwan, R.O.C.
[c]Center for Measurement Standards, Industrial Technology Research Institute, Taiwan, R.O.C.

Abstract

A multi-functional microscope named Morphinscope, which was designed to switch between various measurement functions by simply rotating its turret or turning on some sub-systems, was presented. Some of the various built-in functions of this microscope, including a confocal microscope, a photon-tunneling microscope, a laser based phase-shifting interferometry microscope, a Linnik interference microscope, and an ellipsometer, etc. are examined. The opportunity to bring traceability to thin-film or nano-materials metrology, which is an issue under extensive investigations now, offered by the multi-functional microscope were also detailed. Design thinking, optical and opto-mechanical configurations adopted, and experimental results of this newly multi-functional microscope were examined. Measurement of a grating surface, the real and the imaginary complex refractive indices, and the corrected surface profile of an inhomogeneous specimen were used to demonstrate the performance and advantages of this type of multi-functional microscope. Potential to achieve and transfer traceability of the primary standard in Morphinscope was also discussed.

Keywords: multifunctional microscope, phase-shifting , traceability, confocal microscope, photon-tunneling microscope

1. Introduction

To measure systems of very small size such as semiconductor devices, micro-electro-mechanical systems (MEMS), and Bio-MEMS, optical microscope technology plays a very important role in analyzing specimen surfaces. The lateral resolution of far-field optical microscope is limited by optical diffraction, which means no image with resolution higher than that of the diffraction limit can be obtained. To overcome this problem, techniques such as confocal microscopy [1], two photon microscopy, etc. have been developed. A recent technique based on imposing spatial fringes of different phases onto original image offers another potential possibility [2].

As optical microscopes do not require specially prepared specimen and typically will not cause any harm or damage to the specimen, optical microscopes continue to gain wider popularities despites the invetion and development of many more recent metrology techniques. To further extend the popularity for traditional optical microscopes, many adaptations have

*Corresponding : Wen-Jong Chen, Ph.D. Candidate, National Taiwan University, Dept. of Mechanical Engineering, No. 1, Sec. 4, Roosevel Road, Taipei, Taiwan, Tel/Fax: (+886) 2 2365-9436, e-mail: wjchen@mems.iam.ntu.edu.tw;

been developed over the last two decades to overcome some of the inherent drawback of traditional optical microscopes. The motivation of developing a multi-functional microscope detailed in this article is to construct a single optical test system that possesses versatile metrology functions, and to investigate the possibility of circumventing the diffraction limit in order to achieve higher lateral resolution for traditional optical microscopes. The newly developed multi-functional microscope takes a low cost reflective optical microscope as a basic vehicle to integrate versatile metrology functions such as that of a confocal microscope, a photon tunneling microscope, a laser based phase-shifting interferometry microscope, and an ellipsometer, etc. One of the fundamental reasons for developing this type of microscope lies on the understanding that a major limitation for today's microscope is not only on the resolution but also on the need to use multiple metrology techniques to evaluate the same site of interest in order to gain full understanding of the samples. The lateral need simply cannot be achieved by using different microscopes to investigate the same specimen.

A traditional laser based phase-shifting interferometry microscope is used to measure the surface profile of the specimen by phase shifting method and by phase-reconstruction algorithms. However, if the surface is non-homogeneous, it will introduce erroneous phase shifts by reflection from different materials, which will then lead to incorrect surface profile by using the measured phase diagram. In general, a phase-shifting interferometry microscope is thus used to measure homogeneous surface profiles. Even though several research papers proposed various methods with an intention to correct the phase changes due to reflection from different materials, this article will propose a technique that combines an ellipsometer with a phase-shifting interferometry microscope to reconstruct and obtain the correct surface profile of inhomogeneous specimen.

2. The Mutli-functional microscope

2-1. Photon Tunneling Microscope

The photon tunneling effect occurred at the interface of total internal reflection. Considering the case that light is incident from medium 1 of reflective index n_1 to medium 2 of reflective index $n_2 < n_1$ and the incident angle is larger than the critical angle $\theta_c=sin^1(n_2/n_1)$, the case of the total internal reflection, the wave in medium 2 can be expressed [3]

$$E_{evanescent}(z)=E_0\exp\left(-z/d_p\right)\exp\left[i\left(K_{2z}x-\omega t\right)\right] \tag{1}$$

where E_0 is the magnitude of the wave at the interface of medium 1 and medium 2, d_p is the effective transmitted depth, z is the penetration depth, K_{2z} is the z-component of the refractive wave, ω is the incident light frequency. Equation (1) implies that there is an evanescent field moving along the *x* direction and its magnitude decreases exponentially (Fig.1). When there is an additional medium of refractive index $n_3>n_2$, a phenomenon called *frustrated total internal reflection* will have the evanescent wave propagate through medium 3. If the surface of medium 3 has lateral or longitudinal variations and it is an isotropic and homogeneous material, the reflected wave in the interface of medium 1 and medium 2 will change correspondingly. By measuring the variation of the intensity of the reflected wave, a gray-scale image of the surface profile of the specimen can be obtained [3]. In fact, replacing the microscope objective with an oil lens without put in the oil and then measure the data from CCD will in fact create a photon-tunneling microscope.

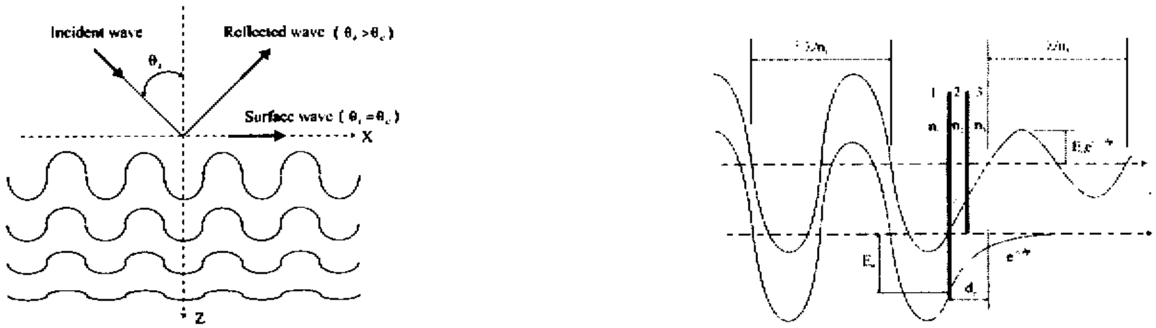

(a) (b)

Figure 1: Illustration of the evanescent field in the presence of the total internal reflection (a), and the variation of the evanescent field magnitude along the z direction (b).

Since the gray scale changes with the surface profile exponentially, the photon-tunneling microscope is much more sensitive than that of the confocal microscope along the z-direction. More specifically, the surface profile z can be obtained by performing logarithmic operations to the intensity map obtained by a photon-tunneling microscope. However, to measure the surface profile quantitatively, many of the constants listed in Eq. (1) must be calibrated in order to ensure traceability in the long run.

2-2. Confocal Microscope

The image recorded from a confocal microscope (Fig. 2) can be derived from the confocal imaging theory, i.e., the intensity measured by the photo detector at the origin of the radial direction can be expressed as [2]

$$I = \left|(h_1 h_2) \otimes T\right|^2 \tag{2}$$

$$I(u,0) = \left|\int_0^{2\pi}\int_0^1 P(\rho,\theta)P(\rho,\pi-\theta)\exp\left(ju\rho^2\right)\rho d\rho d\theta\right|^2 = \left|\int_0^1 \exp\left(ju\rho^2\right)\rho d\rho\right|^2 = \left[\frac{\sin(u/2)}{u/2}\right]^2 \tag{3}$$

where u is the coordinate of the axial direction. It is clear from Eq. (1) that little variations in the axial direction will result in significant fluctuation of intensity $I(u,0)$. More specifically, when the photo detector is located right in the image plane, maximum intensity can be obtained. In other words, when the specimen is in the focal plane of the objective, the reflective light from the specimen will focus in the plane of the pinhole. If the specimen moves out of the focal plane of the objective, a defocus point will form in front of the pinhole; at this time, the intensity measured by the photo detector will be greatly attenuated. This phenomenon can be used to perform optical sectioning of a specimen under observations. In fact, optical sectioning, higher spatial resolution, and shorter depth of focus are the basic and advantageous concepts of confocal microscope [1].

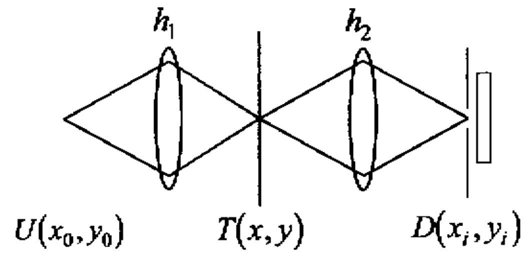

Figure 2: The illustration of optical field of the confocal microscope, where light source $U_0(x_0,y_0)$ is in plane (x_0,y_0), $D(x_i,y_i)$ is the intensity received by the photo detector at plane (x_i,y_i).

2.3 The Morphinscope

The multi-functional microscope termed *Morphinscope* was originally developed to integrate the two above-mentioned microscopes into the Linnik interference microscope. Later on, *Morphinscope* was further designed and developed to perform versatile metrology functions with a vision to switch between its various measurement functions by simply rotating its turret or turning on some sub-systems.

The Linnik interference microscope can measure the sample surface profile by interferometry, and phase shifting techniques can be used to increase the measurement resolutions of interference microscope [4]. As it was mentioned above, the photon-tunneling microscope must go through sample calibration in order to retrieve quantitative data, a microscope that possess all of above functions can certainly have a built-in calibration capability. When adopting interference microscope to measure inhomogeneous surfaces, the extra phase delay induced by reflection from different materials will create erroneous data. An ellipsometer [5] can be used to solve this problem by measuring the refractive index at each specific point of the sample in order to correct this extra phase delay [4].

After the laser light passes thrugh the aperture, it meets up a polarization beam splitter (PBS) first (Fig. 3). The polarized light beam passes through a liquid crystal variable retarder made by Meadowlark Optics, Copr., which was used to control the phase difference between the fast and the slow axes by using the externally applied voltage. The phase modulated light then passes through another 50% non-polarization beam splitter (NPBS1) to have one light beam propagates towards the microscope. The light reflected by NPBS1 is further divided into two light beams. The light detected at detector 3 can in fact be used to normalize any intensity variations induced by the liquid crystal retarder, the laser source itself, etc. For the light beam that enters into the microscope, the light is further divided into three beams by non-polarization beam splitters NPBS2 and NPBS3. The interference image created by the light beam reflected from the sample and the light beam reflected through and back from NPBS3 is in fact a surface profile data measured by using the Linnik type interference microscope. The data obtained from the light reflected from the sample and further reflected from NPBS3, i.e., the data measured at detector 2, is in fact a confocal microscope image. Modulating the retardance by using the liquid crystal retarder, blocking the light beam reflected from NPBS3 and compares the data measured at detector 1 and the CCD image form a phase modulated ellipsometer [5]. More specifically, the Fresnel equation and the Snell's law can be introduced to measure the relative refractive index as each data within the CCD camera in fact represents data induced by light beams from different incident angles. Considering the complex refractive index N,

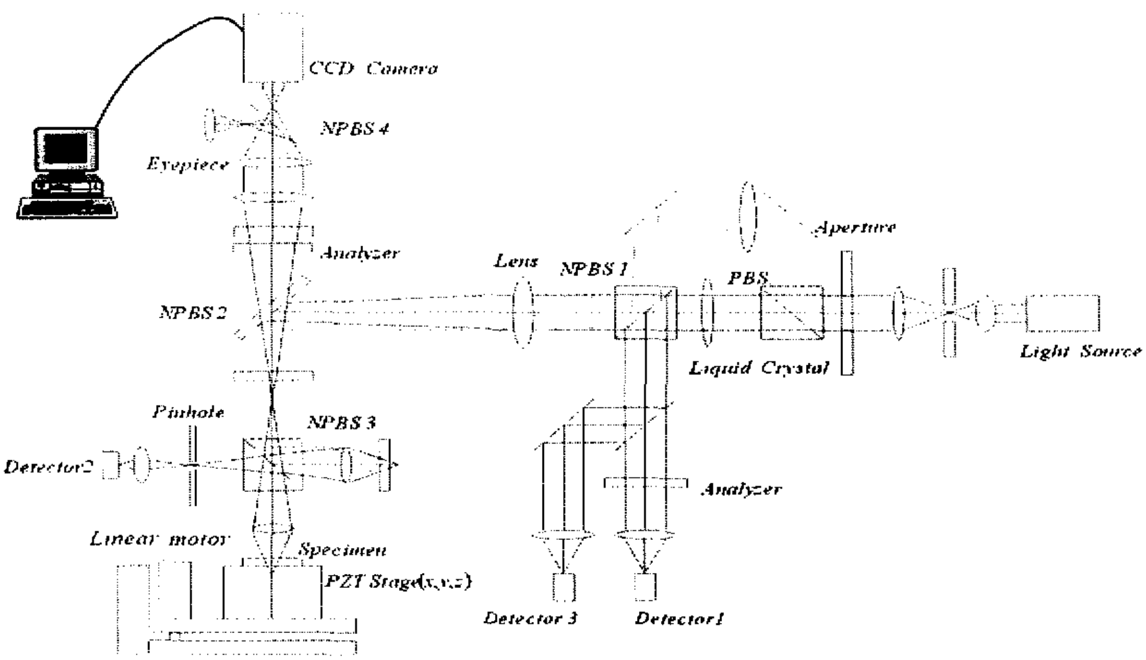

Figure 3: Schematics of the *Morphinscope*.

$$N = n - ik \tag{4}$$

$$r_p = \frac{E_{rp}}{E_{ip}} = \frac{\left[n_r^2 - k_r^2 - i(2n_r k_r)\right]\cos\phi_i - \sqrt{(n_r^2 - k_r^2 - \sin^2\phi_i) - i(2n_r k_r)}}{\left[n_r^2 - k_r^2 - i(2n_r k_r)\right]\cos\phi_i + \sqrt{(n_r^2 - k_r^2 - \sin^2\phi_i) - i(2n_r k_r)}}$$

$$r_s = \frac{E_{rs}}{E_{is}} = \frac{\cos\phi_i - \sqrt{(n_r^2 - k_r^2 - \sin^2\phi_i) - i(2n_r k_r)}}{\cos\phi_i + \sqrt{(n_r^2 - k_r^2 - \sin^2\phi_i) - i(2n_r k_r)}}$$

$$r_p = r_p e^{j\delta_{rp}}, r_s = r_s e^{j\delta_{rs}} \tag{5}$$

where n is the refractive index, k is the extinction coefficient, r_p and r_s are the reflection coefficients of TM wave and TE wave, δ_{rp} and δ_{rs} are phase changes of TM and TE waves. For a monochromatic plane wave incident to an isotropic structure, the ellipsometric function ρ is defined as [5]

$$\rho = \frac{r_p}{r_s} = \tan\psi \exp(j\Delta) \tag{6}$$

where Ψ and Δ are ellipsometric angles of the structure that satisfy the following equation

$$\begin{aligned} \tan\psi &= |r_p| / |r_s| \\ \Delta &= \delta_{rp} - \delta_{rs} \end{aligned} \tag{7}$$

Once the ellipsometric angles are measured, the complex index of refraction N can be retrieved to calculate the correct phase changes due to the reflection. Once the phase error due to reflection of non-homogeneous surfaces is corrected, the interference data obtained can be corrected to become sample surface profile data.

3. Experimental results

First, a 3D surface profile of a specimen was measured by using the confocal microscope and the photon tunneling microscope subsystems of the *Morphinscope* shown in Fig. 3. A 50X objective with numerical aperture 0.75 and a pinhole of $5\mu m$ diameter was used first to perform the confocal measurement. The confocal microscope data shown in Fig. 4(a) is a 4-step reflective grating with a $32\mu m$ period. A total of 961 data points were taken and the spacing of each data point is $0.533\mu m$. The same diffractive grating measured by atomic force microscope (AFM) is shown in Fig. 4(b). The good agreement of the experimental data shown in Fig. 4 confirms the accuracy of the data obtained by the confocal microscope subsystem.

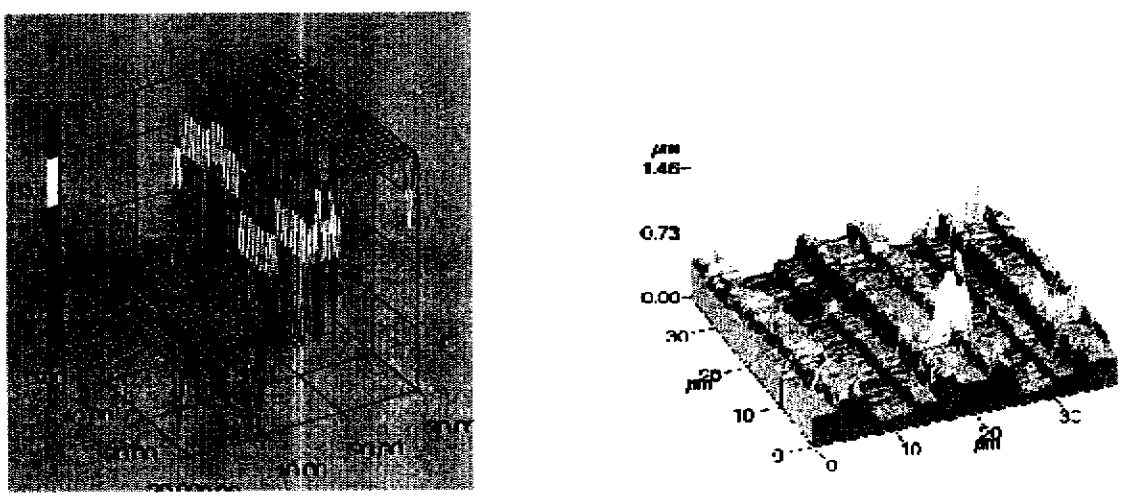

(a) (b)

Figure 4 : Diffractive grating image measured by the confocalm icroscope subsystem of *Morphinscope* (a) and by AFM (b).

Figure 5 shows data obtained by using the photon-tunneling microscope subsystem of the *Morphinscope*. Perform logarithmic function calculations to the gray-scale image of the four-steps diffractive grating with $32\mu m$ period results in the surface profile of the grating. It should be noted that the height of the grating profile is adjusted by multiplying a constant to the measurement data, as photon-tunneling microscope image must be calibrated to arrive at the correct height data. Figure 6 shows the 3D profile of a concave surface obtained by using the Linnik interference microscope subsystem of the *Morphinscope*, which adopts digital cosine transform (DCT) [6] to unwrap the phase map obtained by performing a five step phase shifting algorithm [7]. The refractive indices of a sample surface measured by using the ellipsometer subsystem of the *Morphinscope* are shown in Fig. 7.

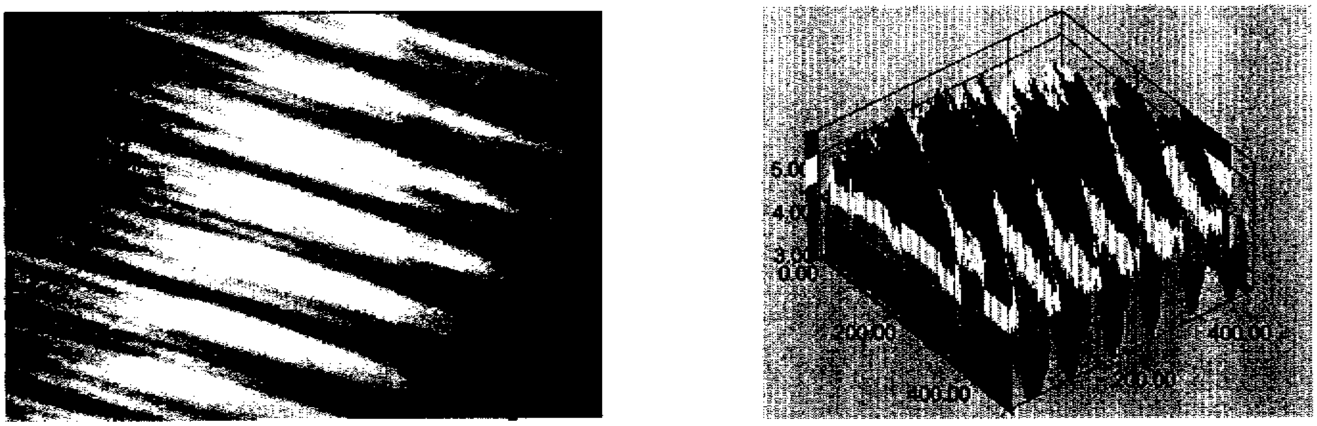

(a) (b)

Figure 5: The intensity map (a) measured by using the photon-tunneling microscope subsystem of the *Morphinscope* was used by retrieve the 3D surface profile (b) of the diffractive grating

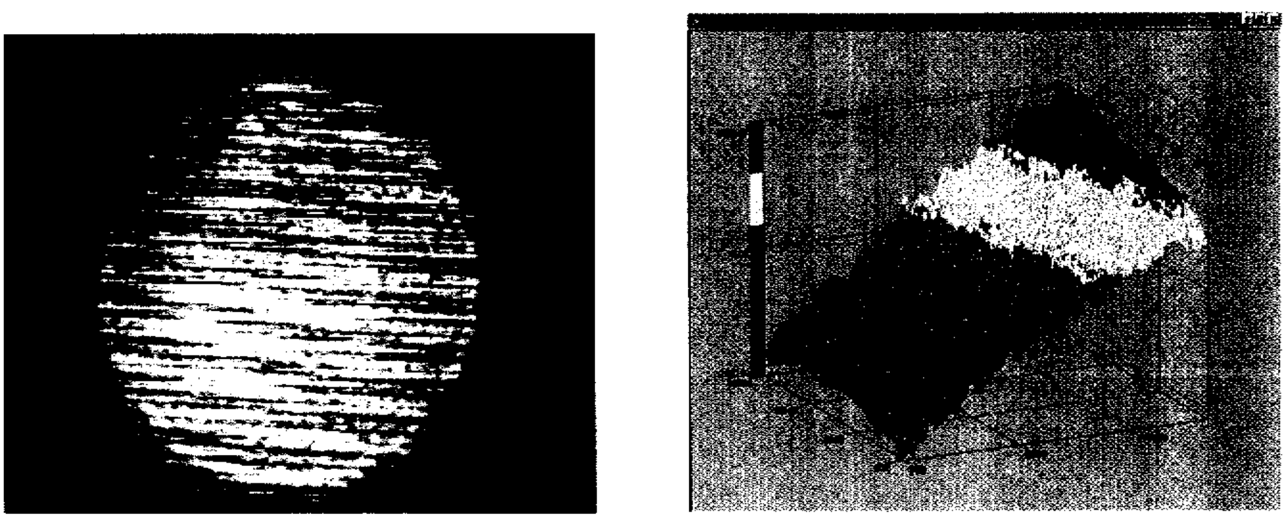

(a)

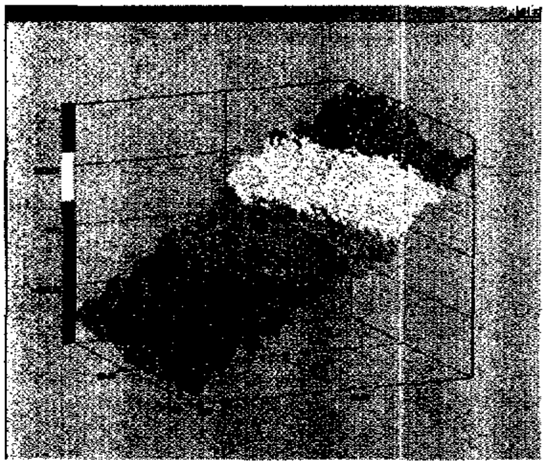

(b)

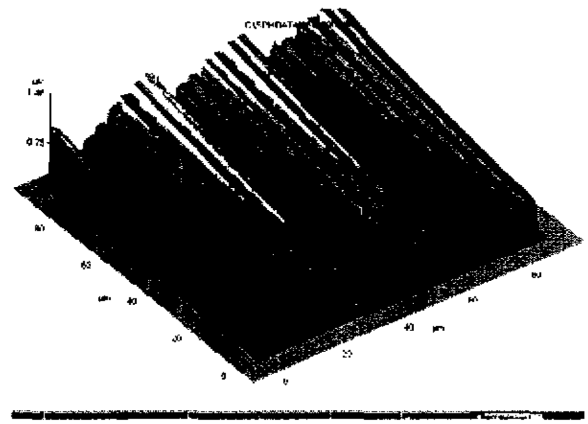

(c)

Figure 6: A grating surface measured by using the Linnik interference microscope subsystem of the *Morphinscope*, where each pixel along the z-axis is 0.5nm and each pixel along the x-axis is 204.375nm, and the y-resolution is 203.750 nm. (a) is before filter , (b) is after filter and (c) is measured by AFM.

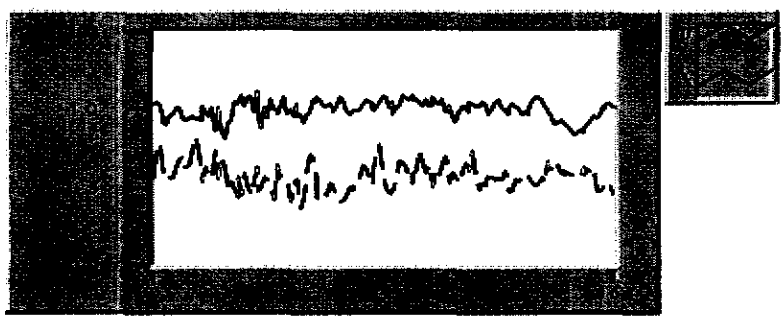

Figure 7: Measurement results of the ellipsometer of the multi-functional microscope (y-axis: rad, x-axis: pixel)

3. Calibrations and traceability

Reference methods and certified reference materials are the grounds of the metrological traceability (Fig. 8)[8]. A reference method can be used to assign a certified value to a reference material and also to validate routine metrology methods. The reference material and validated routine methods can be used in thin-film or nano-materials (Fig. 9) to assign value for commercial calibration. The obtained value will then become traceable to the primary certified reference material in all calibrations.

In the series of calibrations and measurements through the traceability chain (Fig. 8), if the components of the calibration and of the sample measured are identical, then the estimate of concentration is independent of the measurement procedures [8] between the calibration material and the sample. It is clear from the configuration shown in Fig. 3 and the discussions on the various metrology functions of the Morphinscope that traceability can potentially be transferred from the various functions. Since all of the above-mentioned metrology functions were derived from complete different principles, its sensitivity will be different from different linear scale as well. Taking a proper reference material such as the one shown in Fig. 9 and then perform the routine metrology methods to transfer the certified value of the primary standard can then potentially be performed in the newly developed Morphinscope.

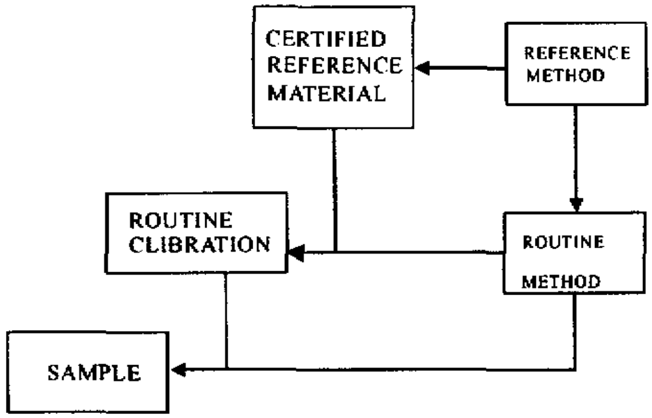

Figure 8: Calibration and traceability scheme

Figure 9: Thin film material of very 40 nm thickness developed to perform traceability of the Morphinscope

4. Conclusions

The *Morphinscope*, that combines the capabilities of a confocal microscope, a photon-tunneling microscope, a Linnik interference microscope, and an ellipsometer, etc. was developed. The confocal microscope and photon tunneling microscope subsystems of this multi-functional microscope was shown to be able to enhance the resolution of typical optical microscope in the height direction and the lateral resolution. The potential to integrate the Linnik interference microscope and the ellipsometer to measure the surface profile of inhomogeneous specimens was also discussed. Potentials to use the various subsystems of the *Morphinscope* to perform cross-calibrations and to explore or investigate interesting sites on the specimen were also detailed. Per the procedure of traceability, it was discussed that the full system integration of Morphinscope can provide us with an opportunity to bring traceability to the metrology of thin film or nano-material for future work.

5. References

1. J. B. Pawley, *Handbook of Biological Confocal Microscopy*, 2nd edition, Plenum Press, New York (1995).
2. G. E. Cragg, and P. T. C. So, "Lateral resolution enhancement with standing evanescent waves" *Opt. Lett.*, Vol. 25, No.1, pp.46- 48 (2000)
3. J. M. Guerra, "Photon Tunneling Microscope," *Applied Optics*, Vol. 29, No. 26, pp. 3741-3752 (September 1990).
4. E. W Rogala, and H. H. Barrett, "Phase-shifting interferometer/ellipsometer capable of measuring the complex index of refraction and the surface profile of a test surface," *J. Opt. Soc. Am. A*, Vol. 15, No. 2, pp. 538 –548 (February 1998).
5. R. M. A. Azzam, and N. M. Bashara, *Ellipsometry and Polarized Light*, North-Holland Publishing Company, New York (1977).
6. D. C. Ghiglia, and L.A. Romero, "Robust Two-dimensional Weighted and Un-weighted Phase Unwrapping That Uses Fast Transforms and Iterative Methods," *J. Opt. Soc. Am. A.*, Vol. 11, pp. 107-117 (1994).
7. C. W. Chen, H. Y. Chang, and C. K. Lee, "An Innovative Phase Shifting System for Non-Destructive Testing," *The Chinese Journal of Mechanics*, Vol. 14, pp. 31-39 (1996).
8. F.Javier Gella, Francesca Canalias "Calibration and traceability of enzyme and antibody measurements," *Clinica Chimica Acta* , Vol. 278, pp. 145-149(1998)

A POSITION DETECTION APPARATUS FOR ULTRA PRECISION MACHINE APPLICATIONS

C.C. Wu
Department of Mechanical Engineering
National Taiwan University
Taipei 10617, Taiwan

C.K. Lee
Institute of Applied Mechanics
National Taiwan University
Taipei 10617, Taiwan

C.T. Hsieh
AHEAD Optoelectrics, Inc.
Taipei Hsien 235, Taiwan

S.S. Lu
Department of Mechanical Engineering
National Taiwan University
Taipei, 10617 Taiwan

ABSTRACT

This paper presents a laser linear encoder, which serves as a position detection apparatus for precision machine applications and can provide a measuring resolution less than 1 nm. It adopts a single-armed 1-x telescope design, which can increase 6 to 20 times of head-to-scale tolerance than existing encoders of the same class. It was identified that this newly proposed laser encoder design could avoid the effect of differences in polarization diffraction efficiencies for the grating scale used. Optimizing the system performance by cleverly designing the profile of the grating scale was also detailed. The effect of non-uniform temperature field within the head-to-scale range that can yield a nonzero initial phase so as to decrease the system measurement accuracy was analyzed. In addition, misalignment of the polarizers located in front the photodiodes were identified to be the main cause for imperfect Lissajous circles, which may lower the measuring resolution when traditional arctangent algorithm was adopted for circular polarization interferometers. The resolution of the newly developed laser encoder was verified by experiments and was found to agree well with the theoretical predictions.

1. INTRODUCTION

Laser encoders, which provide accurate linear and angular displacement information with resolution down to the nanometer range, are commonly used in today's high-tech applications. The main bottleneck in making wide applications of the laser encoders lies in the fact that the optical head of a laser encoder must not only be aligned with micrometer precision but also be held to tight tolerance during system operation. As shown in the Fig. 1, there exist five axes of mechanical runout between the optical head and the operating machine. The mechanical runout of the machine that the grating scale was mounted will directly influence the optical signals and thus may lead to erroneous measurement results. The effect of differences in polarization diffraction efficiency usually spoils the measuring results for optical interference systems, which possess gratings [1, 2]. Thus the raise on the manufacture tolerance of the grating is the key to facilitate the system integration easily. Besides, temperature effect has fatal influence on the system measuring resolution and thus the system operating temperature must be controlled within the specific range.

Principles of the optical system design are described in detail herein by describing the optical paths in detail first and then the error analysis of the head-to-scale mechanical runout will be given. Experimental results obtained by comparing the signal output measured by the newly proposed laser encoders with that of a HP™ laser interferometer are to be examined as well.

2. AN INNOVATIVE OPTICAL HEAD

An innovative optical head is shown in the Fig. 2. A linearly polarized light emitted from the diode laser is collimated and aligned to make sure that the two light beams splitted by the polarization beam splitter (PBS) will have equal intensity. After p-wave (TM wave) transmitting through the PBS and traveling along the left half of the optical path, the quarter waveplate converts the p-wave into a circularly polarized light beam. Similarly the s-wave (TE wave) traveling along the right half of the optical path is converted into a circularly polarized light beam as well. These two orthogonal circularly polarized light beams diffracted by the reflective grating twice are then encoded with the displacement information of the specimen on which the grating is attached.

The *p*- and *s*- polarized light beams are recombined at the PBS. The optical configuration shown in Fig. 2 will make sure that the polarization states of these two light beams are orthogonal to each other. These two orthogonally polarized light beams will become right and left circularly polarized after passing the quarter waveplate. The combination of these two circularly polarized light beams forms effective linearly polarized light beams whose azimuths are functions of the grating displacement. These two polarized light beams produce the quadrature signals from the photodetectors, then the phase decoding algorithm is employed for the signal processing [3, 4]. More specifically, the polarizing plates located in front of the photodetectors PD1 and PD2 are arranged to have a 45° inclined angle with respect to each other within the polarization state space. The light intensities measured by PD1 and PD2 form the quadrature signals, I_1 and I_2, respectively are given by the following equation

$$I_1 = DC_1 + A_1 \cos(\eta), \tag{1}$$

$$I_2 = DC_2 + A_2 \sin(\eta - \delta), \tag{2}$$

where DC_1 and DC_2 are the amplitudes of the DC components, A_1 and A_2 the amplitudes of the AC components, η is the relative phase difference of the two beams due to the displacement of the grating scale, and δ the additional phase difference between the two photo detectors receiving the I_1, I_2 signals. A grating scale displacement of Δx causes a double Doppler shift [5, 6] and which is related to the phase difference η for a first order diffraction by the following equation

$$\eta = 8\pi\Delta x/d, \tag{3}$$

where d is the grating pitch. The phase difference between these two beams depends on the position of the diffraction grating. As the diffraction grating moves, the phase relationships of these two beams change, causing them to constructively or destructively interfere. By Eq. (3), the peak-to-peak period of the interfering beams within the encoder is $d/4$. By interpolation of the quadrature signal electronically, for example, the measuring resolution of the laser encoder system can be improved to better than 0.1 nm with a grating pitch of 1.6 μm and 4096 digitization resolution.

The 1-x telescope design adopted in this optical head can be described by using the matrix optics approach as follows [7]:

$$\begin{bmatrix} 1 & -f \\ 0 & 1 \end{bmatrix}\begin{bmatrix} 1 & 0 \\ 1/f & 1 \end{bmatrix}\begin{bmatrix} 1 & -f \\ 0 & 1 \end{bmatrix}\begin{bmatrix} 1 & 0 \\ 0 & -1 \end{bmatrix}\begin{bmatrix} 1 & f \\ 0 & 1 \end{bmatrix}\cdot \begin{bmatrix} 1 & 0 \\ -1/f & 1 \end{bmatrix}\begin{bmatrix} 1 & f \\ 0 & 1 \end{bmatrix}\begin{Bmatrix} h_0 \\ \alpha_0 \end{Bmatrix} = \begin{Bmatrix} -h_0 \\ \alpha_0 \end{Bmatrix}, \tag{4}$$

where (h_0, α_0) represents the corresponding position and direction angles of the diffracted beam from the moving grating scale surface, and f is the focal length of the lens as shown in the Fig. 3. By Eq. (4), it can be shown that the output beam, transferred by the 1-x telescope optical system, traces along the opposite direction to the diffracted beam, and its output position located at $-h_0$ is symmetric to the optical axis of the 1-x telescope optical system with the position of the diffracted beam. Thus three advantages for the 1-x telescope can be clearly identified by using the results shown in Eq. (4). Firstly, it assures that a second time diffracted beam can trace along an optical path that is parallel to the original one. Secondly, it provides the returned light beams with offset avoiding the returned beams going back into the laser cavity to de-stabilize the laser. Thirdly, even for the defocused case, which shows up under an additional spacing between the optical head and the grating scale, the output direction of the returned beam can still be held onto an opposite direction that is parallel to its original one. Therefore, this optical design makes the newly developed encoder system more robust than others.

3. ERROR ANALYSIS

The I_1 and I_2 signals trace out a trajectory in the intensity space. The position and shape of the signal trajectory depend on the DC_1, DC_2, A_1 and A_2 levels and thus influence the output accuracy of the signal processing using the arctangent algorithm. The head-to-scale and photodetector module alignment errors will be detailed herein.

Effect of differences in polarization diffraction efficiency

For past laser encoders, errors stemming from the different diffraction efficiency for incident light beams of different polarization states are one of the main design issues [2, 8]. Although Mitutoyo's design claims that it can correct the effect of the differences of the polarization diffraction efficiency [2], it adopts an improper physical concept that the efficiencies of the grating diffraction have reversibility and thus may cause a system measurement error. In comparison, as the proposed laser encoder adopts a circular polarization interferometer configuration and thus is independent of the polarization differences of the diffraction efficiency, the quadrature signals are of the same amplitude. It can be shown clearly that incident light beams after twice diffractions from the grating scale

(Fig. 2) lead to a resultant electric field E located in front of the second NPB that consists of a left-circularly and a right-circularly polarized components with the same amplitude. The corresponding quadrature signal can be shown as follows

$$I_1 = DC + AC \cdot \cos(4 \cdot \Delta\omega \cdot t), \quad (5)$$

$$I_2 = DC + AC \cdot \sin(4 \cdot \Delta\omega \cdot t), \quad (6)$$

where DC, AC are the amplitudes of the DC, AC components of the quadrature signal respectively, and

$$AC = G[k_p(\theta)k_p(0) + k_s(\theta)k_s(0)]^2 \quad (7)$$

$$DC = G[k_p(\theta)k_p(0) + k_s(\theta)k_s(0)]^2 \quad (8)$$

where G is a proportional constant, $\Delta\omega$ is the Doppler angular frequency shift and the $k_p(\theta)$, $k_p(0)$, $k_s(\theta)$ and $k_s(0)$ are the first order diffraction efficiencies with respect to the θ and 0 incident angles for p- and s-polarizations respectively. From Eqs. (5-8), it is clear that the optical design of the newly developed laser encoder does not distort the output signal and the output resolution of the phase decoding is free from the effect of differences in the diffraction efficiencies for incident light beams with different polarization states. That is, the laser encoder remains in optimum operating condition even for the cases that the difference in diffraction efficiencies exists for incident light with different polarization states.

Effect of temperature

It is very difficult to keep this system temperature completely balanced; i.e. the OPD does exist between *path1* and *path2*, which are optical paths respectively along the left and right half of optical paths. Temperature variation influences the measurement accuracy with an additional phase γ for the phase decoding and it can be shown easily by using Jones calculus as follows

$$\eta = 4 \cdot \Delta\omega \cdot t + \gamma \quad (9)$$

where t is the time interval during the grating scale movement, γ, the temperature variation induced phase error can be represented as follows

$$\gamma = \frac{4\pi}{\lambda}\left[\int_{path1} \Delta n \cdot dl - \int_{path2} \Delta n \cdot dl\right] \quad (10)$$

where λ is the wavelength of the laser source, Δn is the index change induced by the temperature variation within the optical system with respect to the standard ambient temperature 20°C, dl is the infinitesimal path along *path1* or *path2* and

$$\Delta n = n(x,z) - n_0 \quad (11)$$

where $n(x, z)$ is the index distribution caused by the temperature variation, and n_0 is the reference index at 20°C constant ambient temperature. Out of the laser encoder, only the head-to-scale region is exposed directly to the ambient environment and thus we can reasonably assume that the region within the optical head has a uniform temperature field. For example, consider a head-to-scale region of 1mm spacing, *path1* with a uniform temperature variation, *path2* with the same temperature as the reference temperature, 20°C, which is the ambient temperature and a laser source with a wavelength at 633nm. By Eqs. (9-11) and the empirical refractive index formula which is a function of temperature variation [9], we can estimate an error sensitivity of the displacement measurement, 1.1721nm/°C as shown in the Fig. 4. Thus the temperature variation is radically significant for the measurement accuracy of the laser encoder system.

The polarization misalignment of the detector modules

It should be noted that errors do occur when the two PBSs in front of the corresponding photodetectors are misaligned at wrong relative polarization angles. By Jones calculus the misalignment angle ξ can be related to the polarization misalignment error which shows up as an additional phase difference δ in the quadrature signals in Eq. (2), and

$$\delta = 2 \cdot \xi. \quad (12)$$

Especially the polarization misalignment $\varepsilon(\eta)$ at detector modules induced error is a periodic error with respect to the phase η of the quadrature signal. As the arctangent algorithm is applied, the error $\varepsilon(\eta)$ can be easily written down as follows

$$\varepsilon(\eta) = \tan^{-1}\left[\frac{\sin(\eta - \delta)}{\cos\eta}\right] - \eta, \quad (13)$$

and

$$\varepsilon(\eta + \pi) = \varepsilon(\eta) \quad (14)$$

By Eq. (14), it is clear that the polarization misalignment at the detector modules does induce an error with a period π. Since this error is periodic, it can improve the resolution of the system down to near 1pm for the corresponding quadrature signal processing by using the periodic average technique [10]. Even for the additional phase difference of one degree, which is equivalent to an angle difference of 0.5° stemming from the polarization misalignment of the detector module, there will exist a displacement measurement error larger than 1 nm and make the measurement failed as shown clearly in the Fig. 5.

The head-to-scale mechanical runout

For the system shown in Fig. 1, the roll and yaw is the runout that is most difficult to minimize due to the nature of the stage movement. That is, the high-speed motion of the stage naturally leads to high roll and yaw runout. It is clear from the data shown in Table 1 that the newly developed laser encoder improves the most critical runout by a factor of 6 to 20. This significant improvement leads to a laser encoder that is much easier to implement and has a much higher performance.

4. EXPERIMENTAL RESULTS

The laser encoder system is calibrated using a HP5529A interferometer and the experimental setup is shown in the Fig. 6. To further verify the performance of the newly developed laser encoder, same stage movement was measured by using the laser encoder as well as the HP™ 5529A distance measuring interferometer. The data obtained were shown in the Fig. 7. The experimental data obtained clearly demonstrates the performance of this newly developed laser encoder. The discrepancy between the signals obtained from the laser encoder and the HP interferometer can be traced to the oscillations of the mounting fixtures that hold the optical components of the table-top laser encoder presented. It is expected that the performance will be significantly improved either by enhancing the mounting fixtures or by setting up a laser encoder prototype in the near future.

5. CONCLUSIONS

A linear laser encoder that adopts the 1-x telescope concept was developed to provide a solution to counter the errors induced by practical mechanical runout of the specimen. The optical principle and the design thinking of this newly developed system were also examined. Influence of laser encoder performance by the grating characteristics including the incidence angle, the surface profile, the grating depth, etc. was also detailed. The error from the grating diffraction efficiency discrepancy of the incident light beams of different polarization states was evaluated. The effect of temperature and the polarization misalignment of the photodetectors are very important for the measurement accuracy and resolution. It was identified that the grating scale should be viewed as a fundamental parameter of the optical design for linear laser encoders. The underlying reason that the newly developed laser encoder can have a much better head-to-scale alignment tolerance was also detailed. Experimental data obtained by using both a newly developed tabletop laser encoder and a HP distance measuring interferometer was found to be in good agreement.

ACKNOWLEDGEMENTS

The authors gratefully acknowledge the support of the National Science Council of Taiwan, R.O.C. under the Industrial University Collaborative project numbers: NSC88-2622-E-002-001, NSC88-2622-E-002-002, NSC 85-2622-E-002-017R, and NSC86-2622-E-002-023R.

REFERENCE

[1] Souji, I., Hideki, O. and Seiji S., "Diffraction-type optical encoder with improved detection signal insensitivity to optical grating gap variation," *U.S. Patent No. 4,943,716*.

[2] Masreliez, K.G., "Position detector and method of measuring position," *U.S. Patent No. 5,104,225*.

[3] Lee, C.K., Wu, G.Y., Teng, C.T., Wu, W.J., Lin, C.T., Hsiao, W.H., Shih, H.C., Wang, J.S., Lin S.C., Lin, C.C., Lee, C.F. and Lin, Y.C., "A high performance Doppler interferometer for advanced optical storage systems, *Jpn. J. Appl. Phys.*, Vol. 38, pp. 1730-1741, 1999.

[4] Wu, C.C., Chen, Y.C., Lee, C.K., Hsieh, C.T., Wu, W.J. and Lu, S. S., "Design verifications of a linear laser encoder with high head-to-scale tolerance," SPIE Vol. 3779, pp. 73-82, 1999.

[5] Drain, L.E., The Laser Doppler Technique, John Wiley & Sons, New York, New York, 1980.

[6] Durst, F., Melling, A. and Whitelaw, J.H., *Principles and Practice of Laser Doppler Anemometry*, Academic Press, New York, New York, 1976.

[7] Guenther, R., *Modern Optics*, John Wiley & Sons, New York, New York, 1990.

[8] Hutley, M.C., *Diffraction Gratings*, Academic Press, New York, New York, 1982.

[9] Smith, W.J., *Modern Optical Engineering*, McGraw-Hill, New York, New York, 1990.

[10] G rsel, Y., "Laser metrology gauges for OSI," *SPIE Vol. 1947*, pp. 188-197, 1993.

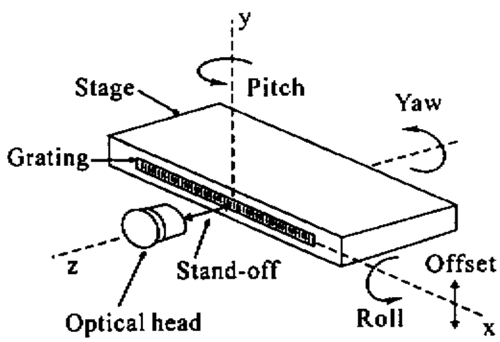

Fig. 1 Schematics of the mechanical runout that may influence the performance of the encoders.

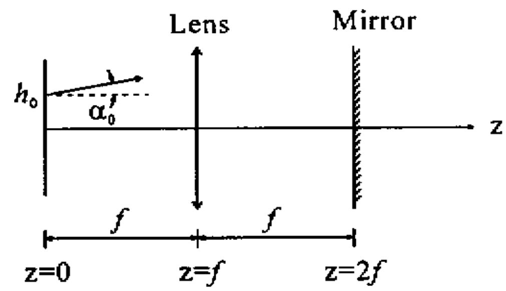

Fig. 3 Schematics of the 1-x telescope.

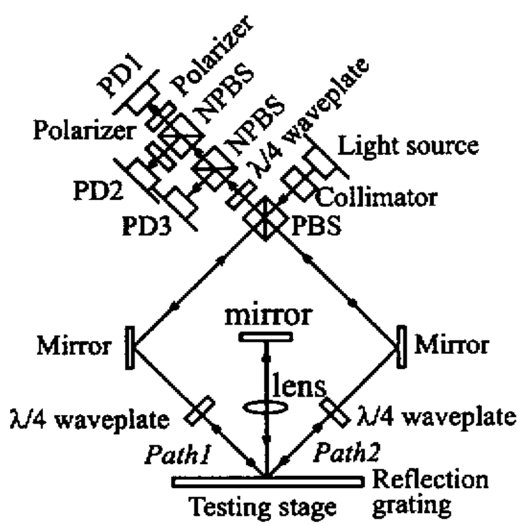

Fig. 2 Schematics of the newly proposed linear encoder.

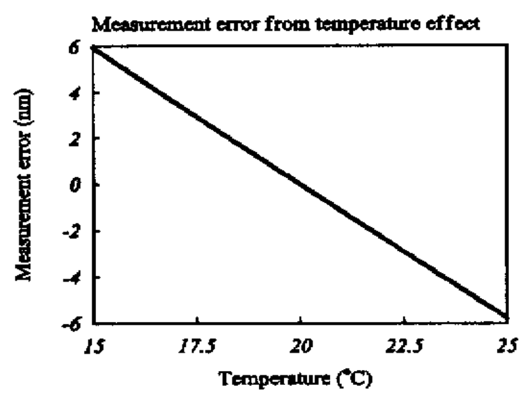

Fig. 4 The optical path difference induced by the difference between the operating temperature and the reference temperature 20°C.

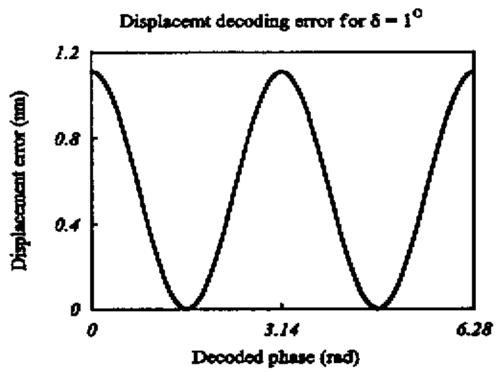

Fig. 5 Displacement error induced by the misalignment of pass axis of the polarizers located in front of the photo detectors.

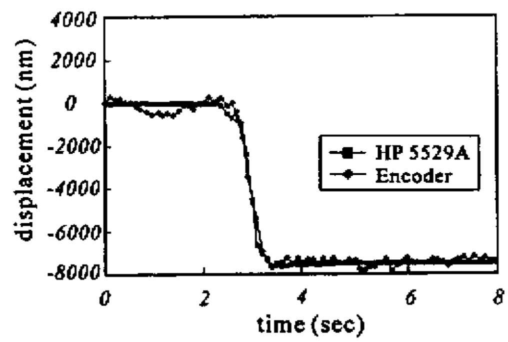

Fig. 7 Comparisons of the measured stage displacement between HP 5529A interferometer and the newly developed laser encoder.

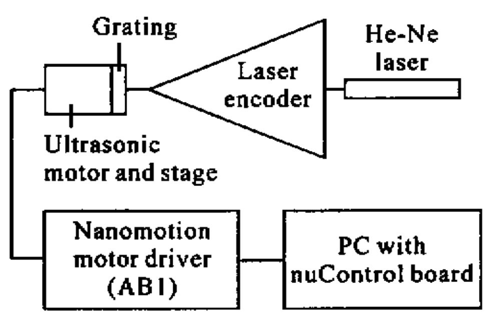

Fig. 6 The experimental setup for the performance test of the laser linear encoder.

A MULTI-FUNCTIONAL MICROSCOPE FOR MEASURING INHOMOGENEOUS SURFACE PROFILE

W. J. Chen
Department of Mechanical Engineering
National Taiwan University
Taipei 10617, Taiwan

C.K. Lee
Institute of Applied Mechanics
National Taiwan University
Taipei 10617, Taiwan

S.S. Lu
Department of Mechanical Engineering
National Taiwan University
Taipei, 10617 Taiwan

ABSTRACT

A newly developed multi-functional microscope system, named *Morphinscope*, that integrates the function of a confocal microscope, a photon tunneling microscope, a laser based phase-shifting interferometry microscope, and an ellipsometer was developed to facilitate the measurement of inhomogeneous surface profile. Design, configurations, and experimental data of this newly developed instrument were all detailed. Combining this understanding, this *Morphinscope* has the possibility of retrieving the surface profile of a non-homogeneous media.

1. INTRODUCTION

The microscope technology has always had the center stage of measuring miniature specimen. With the rapid advancement of micro-optical and microelectronic components, micro-electro-mechanical systems (MEMS), etc., the importance of the microscope is ever more important than before. Even though the resolution of optical microscope is limited by optical diffraction, many add-on technologies such as photon tunneling microscope, near-field optical microscope, etc. have been developed over the years to overcome the diffraction limit. With all these advancements, it was identified that the main bottleneck for today's optical microscope technology was not the resolution. The main limitation actually lies on trying to use the many different microscope based instruments to examine or to explore any specific sites of a specimen. More specifically, once an interesting site was identified, an user typically will need a differnt microscope to measure other properties of the same site. However, the large area ratio between the whole specimen and the specific site makes locating the same site difficult, if not impossible. With an intention to overcomg this problem, a multi-functional microscope that possesses versatile metrology functions and wide test capabilities/ranges within a single instrument was developed. It was identified that this type of multi-functional microscope not only saves the cost, but also has many built-in calibration and new-found capabilities that were not available before the development of such multi-functional microscope. Since this type of microscope can *morph* form one configuration to another, it was named *Morphinscope*.

The *Morphinscope* to be presented herein was developed by using a low cost reflective optical microscope as the basic platform and has integrated versatile metrology functions such as that of a confocal microscope, a photon tunneling microscope, a laser based phase-shifting interferometry microscope, and an ellipsometer. As it was mentioned above, many new-found capabilities were available in this type of instrument. For example, a traditional laser based phase-shifting interferometry microscope can only be used to measure the surface profile of a homogeneous specimen as optical phase was the fundamental parameter that was measured and different material will induce different phase retardation during reflection. Nevertheless, this shortcoming can be circumvented by introducing an ellipsometer to compliment the function of the traditional phase-shifting interferometry microscope to measure inhomogeneous sample surfaces.

2. THEORY

Some of the fundamental theoretical perspectives related to the newly developed *Morphinscope* are to be reviewed herein.

Confocal Microscope

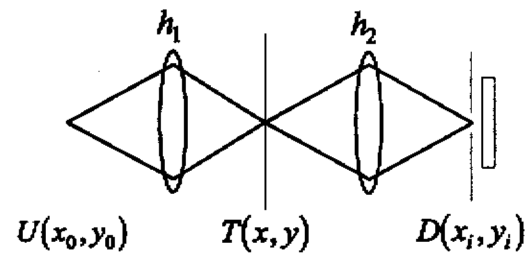

Fig. 1. The illustration of optical field of the confocal microscope, where light source $U_o(x_o, y_o)$ is in plane (x_o, y_o), $D(x_i, y_i)$ is the intensity received by the photo detector at plane (x_i, y_i).

The image recorded from a confocal microscope (Fig. 1) can be derived from the confocal imaging theory, i.e., the intensity measured by the photo detector at the origin of the radial direction can be expressed as [1]

$$I(u, 0) = [\sin(u/2)/u/2]^2 \quad (1)$$

where u is the coordinate of the axial direction. It is clear from Eq. (1) that little variations in the axial direction will result in significant fluctuation of intensity $I(u, 0)$. More specifically, when the photo detector is located right in the image plane, maximum intensity can be obtained. In other words, when the specimen is in the focal plane of the objective, the reflective light from the specimen will focus in the plane of the pinhole. If the specimen moves out of the focal plane of the objective, a defocus point will form in front of the pinhole; at this time, the intensity measured by the photo detector will be greatly attenuated. This phenomenon can be used to perform optical sectioning of a specimen under observations. In fact, optical sectioning, higher spatial resolution, and shorter depth of focus are the basic and advantageous concepts of confocal microscope [1].

Photon Tunneling Microscope

The photon tunneling effect occurrs at the process of total internal reflection. Considering the case that light is incident from medium 1 of reflective index n_1 to medium 2 of reflective index $n_2 < n_1$ and the incident angle is larger than the critical angle $\theta_c = \sin^{-1}(n_2/n_1)$, i.e., the case of the total internal reflection, the wave in medium 2 can be expressed [2]

$$E_{evanescent}(z) = E_0 \exp(-z/d_p) \exp[i(K_{2z} x - \omega t)] \quad (2)$$

where E_0 is the magnitude of the wave at the interface of medium 1 and medium 2, d_p is the effective transmitted depth, z is the penetration depth, K_{2z} is the z-component of the refractive wave, ω is the incident light frequency. Equation (2) implies that there is an evanescent field moving along the x direction and its magnitude decreases exponentially (Fig.2). When there is an additional medium of refractive index $n_3 > n_2$, a phenomenon called *frustrated total internal reflection* will have the evanescent wave propagate through medium 3. If the surface of medium 3 has lateral or longitudinal variations and it is an isotropic and homogeneous material, the reflected wave in the interface of medium 1 and medium 2 will change correspondingly. By measuring the variation of the intensity of the reflected wave, a gray-scale image of the surface profile of the specimen can be obtained [2]. In fact, replacing the microscope objective with an oil lens without put in the oil and then measure the data from CCD will in fact create a photon-tunneling microscope.

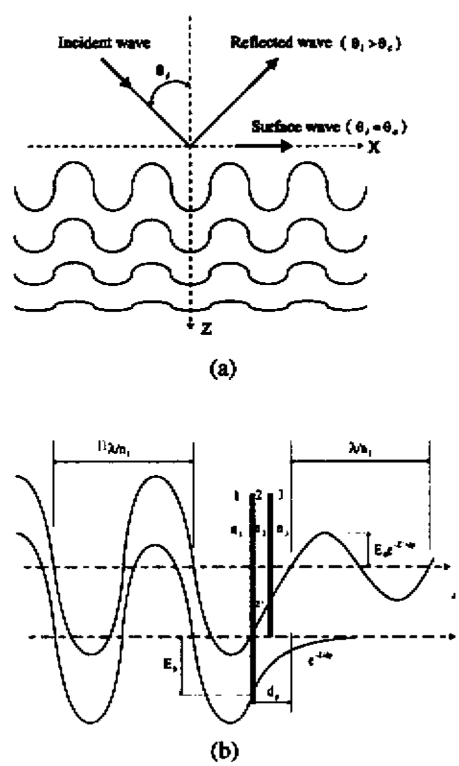

Fig. 2. Illustration of the evanescent field in the presence of the total internal reflection (a), and the variation of the evanescent field magnitude along the z direction (b).

Since the gray scale changes with the surface profile exponentially, the photon-tunneling microscope is much more sensitive than that of the confocal microscope along the z-direction. More specifically, the surface profile z can be obtained by performing logarithmic operations to the intensity map obtained by a photon-tunneling microscope. However, to measure the surface profile quantitatively, many of the constants listed in Eq. (2) must be calibrated.

The Morphinscope

The Linnik interference microscope can measure the sample surface profile by interferometry and phase shifting techniques can be used to increase the measurement resolutions of interference microscope [3]. As it was mentioned above, the photon-tunneling microscope must go through sample calibration in order to retrieve quantitative data, a microscope that possess all of above functions can certainly have a built-in calibration capability. When adopting interference microscope to measure inhomogeneous surfaces, the extra phase delay induced by reflection from different materials will create erroneous data. An ellipsometer [4] can be used to solve this problem by measuring the refractive index at each specific point of the sample in order to correct this extra phase delay [3]. The newly developed multi-functional microscope *Morphinscope* was designed to perform versatile metrology functions and can switch between its various measurement functions by simply rotating its turret or turning on some sub-systems.

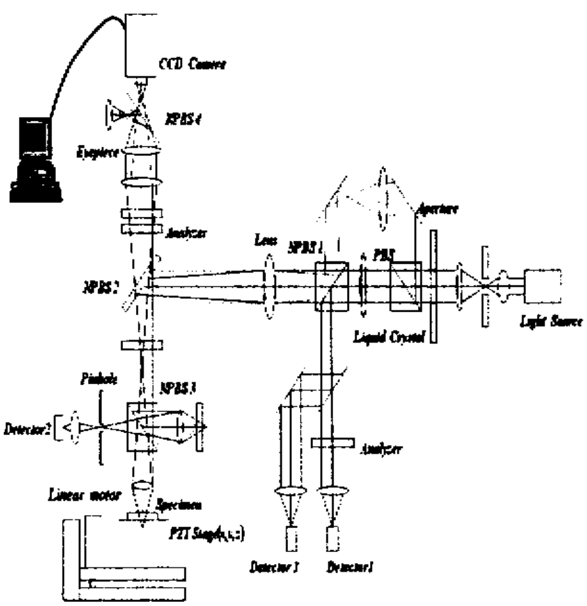

Fig. 3. Schematics of the *Morphinscope*.

After the laser light passes thrugh the aperture, it meets up a polarization beam splitter (PBS) first (Fig. 3). The polarized light beam passes through a liquid crystal variable retarder made by Meadowlark Optics, Copr., which was used to control the phase difference between the fast and the slow axes by using the externally applied voltage. The phase modulated light then passes through another 50% non-polarization beam splitter (NPBS1) to have one light beam propagates towards the microscope. The light reflected by NPBS1 is further divided into two light beams. The light detected at detector 3 can in fact be used to normalize any intensity variations induced by the liquid crystal retarder, the laser source itself, etc. For the light beam that enters into the microscope, the light is further divided into three beams by non-polarization beam splitters NPBS2 and NPBS3. The interference image created by the light beam reflected from the sample and the light beam reflected through and back from NPBS3 is in fact a surface profile data measured by using the Linnik type interference microscope. The data obtained from the light reflected from the sample and further reflected from NPBS3, i.e., the data measured at detector 2, is in fact a confocal microscope image. Modulating the retardance by using the liquid crystal retarder, blocking the light beam reflected from NPBS3 and compares the data measured at detector 1 and the CCD image form a phase modulated ellipsometer [4]. More specifically, the Fresnel equation and the Snell's law can be introduced to measure the relative refractive index as each data within the CCD camera in fact represents data induced by light beams from different incident angles. Considering the complex refractive index N,

$$N = n - ik \tag{3}$$

$$r_p = r_p e^{j\delta_{rp}}, \quad r_s = r_s e^{j\delta_{rs}} \tag{4}$$

where n is the refractive index, k is the extinction coefficient, r_p and r_s are the reflection coefficients of TM wave and TE wave, δ_{rp} and δ_{rs} are phase changes of TM and TE waves. For a monochromatic plane wave incident to an isotropic structure, the ellipsometric function ρ is defined as [4]

$$\rho = \frac{r_p}{r_s} = \tan\Psi \exp(j\Delta) \tag{5}$$

where Ψ and Δ are ellipsometric angles of the structure that satisfy the following equation

$$\tan\psi = |r_p| / |r_s|$$
$$\Delta = \delta_{rp} - \delta_{rs} \qquad (6)$$

Once the ellipsometric angles are measured, the complex index of refraction N can be retrieved to calculate the correct phase changes due to the reflection. Once the phase error due to reflection of non-homogeneous surfaces is corrected, the interference data obtained can be corrected to become sample surface profile data.

3. EXPERIMENTAL RESULTS

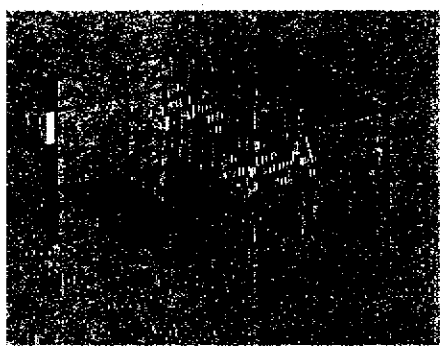

(a)

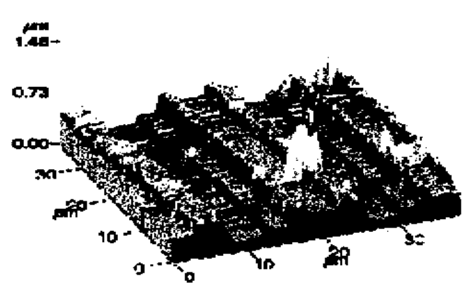

(b)

Fig. 4. Diffractive grating image measured by the confocal microscope subsystem of *Morphinscope* (a) and by AFM (b).

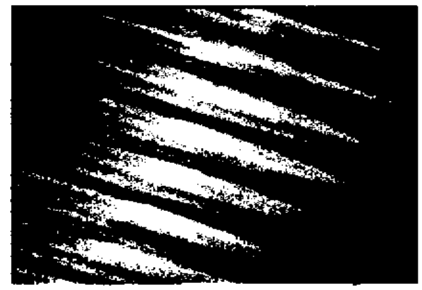

(a)

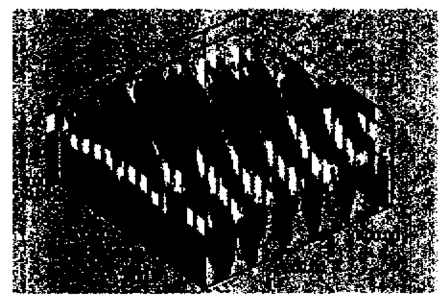

(b)

Fig. 5. The intensity map (a) measured by using the photon-tunneling microscope subsystem of the *Morphinscope* was used by retrieve the 3D surface profile (b) of the diffractive grating.

First, a 3D surface profile of a specimen was measured by using the confocal microscope subsystem of the *Morphinscope* shown in Fig. 3. A 50X objective with numerical aperture 0.75 and a pinhole of 5μm diameter was used. The data shown in Fig. 4a is a 4-step reflective grating with 32μm period. A total of 961 data points were taken and the spacing of each data point is 0.533μm. The same diffractive grating measured by atomic force microscope (AFM) is shown in Fig. 4b. The good agreement of the experimental data shown in Fig. 4 confirms the accuracy of the data obtained by the confocal microscope subsystem. Figure 5 shows data obtained by using the photon-tunneling microscope subsystem of the *Morphinscope*. Perform logarithmic function calculations to the gray-scale image of the four-steps diffractive grating with 32μm period results in the surface profile of the grating. It should be noted that the height of the grating profile is adjusted by multiplying a constant to the measurement data, as photon-tunneling microscope image must be calibrated to arrive at the correct height data. Figure 6 shows the 3D profile of a concave surface obtained by using the Linnik interference microscope subsystem of the *Morphinscope*, which adopts digital cosine transform (DCT) [5] to unwrap the phase map obtained by performing a five step phase shifting algorithm [6]. The refractive indices of a sample surface measured by using the ellipsometer subsystem of the *Morphinscope* are shown in Fig. 7.

Fig. 6. A concave surface measured by using the Linnik interference microscope subsystem of the *Morphinscope*, where each pixel along the z-axis is 0.5nm and each pixel along the x-axis is 204.375nm, and the y-resolution is 203.750nm.

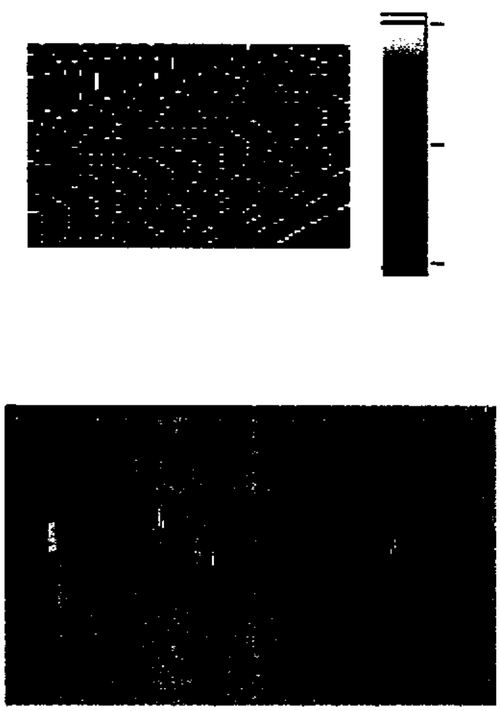

(a)

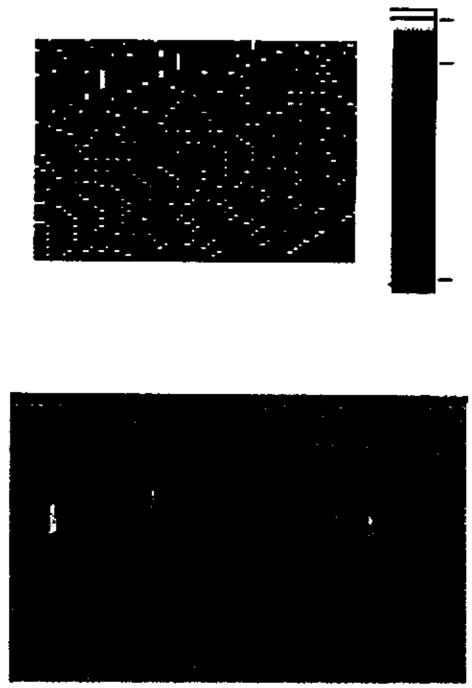

(b)

Fig. 7. The full-field results of a sample surface measured by using the ellipsometer subsystem of the *Morphinscope*, where (a) is the refractive indices and (b) is the extinction coefficients.

4. CONCLUSIONS

A multi-functional microscope, named *Morphinscope*, that combines the capabilities of a confocal microscope, a photon tunneling microscope, a Linnik interference microscope, and an ellipsometer, etc. was developed. The confocal microscope and photon tunneling microscope subsystems of this *Morphinscope* was shown to be able to enhance the resolution of typical optical microscope in the height direction. The potential to integrate the Linnik interference microscope and the ellipsometer to measure the surface profile of inhomogeneous specimens was also discussed. Potentials to use the various subsystems of the *Morphinscope* to perform cross-calibrations and to explore or investigate interesting sites on the specimen were also detailed.

For future work, an ultrahigh precision moiré interferometer was being developed within the configuration of the *Morphinscope* in order to measure the in-plane displacement of the specimen. Nevertheless, it was later discovered that this type of full system integration can provide us with an opportunity to bring traceability to the metrology of thin film or nano-material.

REFERENCES

[1] J. B. Pawley, *Handbook of Biological Confocal Microscopy*, 2nd edition, (Plenum Press, New York, 1995).

[2] J. M. Guerra, "Photon Tunneling Microscope," Applied Optics, 29, 26, 3741-3752 (September 1990).

[3] E. W Rogala, and H. H. Barrett, "Phase-shifting interferometer/ellipsometer capable of measuring the complex index of refraction and the surface profile of a test surface," J. Opt. Soc. Am. A, 15, 2, 538 –548 (February 1998).

[4] R. M. A. Azzam, and N. M. Bashara, Ellipsometry and Polarized Light, (North-Holland Publishing Company, New York, 1977).

[5] D.C. Ghiglia, and L.A. Romero, "Robust Two-dimensional Weighted and Un-weighted Phase Unwrapping That Uses Fast Transforms and Iterative Methods," J. Opt. Soc. Am. A., 11, 107-117 (1994).

[6] C.W. Chen, H.Y. Chang, and C.K. Lee, "An Innovative Phase Shifting System for Non-Destructive Testing," The Chinese Journal of Mechanics, 14, 31-39 (1996).